

Dual-polarization OFDM-OQAM for communications over optical fibers with coherent detection

François Horlin,^{1,*} Jessica Fickers,¹ Philippe Emplit,¹
André Bourdoux,² and Jérôme Louveaux³

¹ Université libre de Bruxelles, Av. Roosevelt 50, 1050 Brussels, Belgium

² Interuniversity Micro-Electronics Center, Kapeldreef 75, 3001 Heverlee, Belgium

³ Université catholique de Louvain, Place du Levant 2, 1348 Louvain-la-Neuve, Belgium

*fhorlin@ulb.ac.be

Abstract: In order to improve the spectral efficiency of coherent optical communication systems, it has recently been proposed to make use of the orthogonal frequency-division multiplexing offset quadrature amplitude modulation (OFDM-OQAM). Multiple optical channels spaced in the frequency domain by the symbol rate can be transmitted orthogonally, even if each channel overlaps significantly in frequency with its two adjacent channels. The solutions proposed until now in the literature unfortunately only address a single polarization communication, and therefore do not benefit from the capacity gain reached when two polarizations are used to transmit independent information signals. The aim of the present paper is to propose a receiver architecture that can decouple the two polarizations. We build an equalizer per channel at twice the symbol rate and optimize it based on the minimum mean square error (MMSE) criterion. We demonstrate the efficiency of the resulting system compared to the Nyquist wavelength-division multiplexing (N-WDM) system both in terms of performance and complexity. We also assess the system sensitivity to transmit synchronization errors and show that system can even work under significant synchronization errors.

© 2013 Optical Society of America

OCIS codes: (060.1660) Coherent communications; (060.2330) Fiber optics communications; (060.4080) Modulation.

References and links

1. S. Tsukamoto, D. Ly-Gagnon, K. Katoh, and K. Kikuchi, "Coherent demodulation of 40Gb/s polarization-multiplexed QPSK signals with 16GHz spacing after 200-km transmission," in *Proc. OFC2005* (Anaheim, U.S.A., 2005).
2. G. Charlet, "Coherent detection associated with digital signal processing for fiber optics communication," *Elsevier, Compt. Rend. Phys.* **9**, 1012–1030 (2008).
3. G. Bosco, A. Carena, V. Curri, P. Poggiolini, and F. Forghieri, "Performance limits of Nyquist WDM and CO-OFDM in high-speed PM-QPSK systems," *IEEE Photon. Technol. Lett.* **22**(15), 1129–1131 (2010).
4. R. Cigliutti, A. Nespola, D. Zeolla, G. Bosco, A. Carena, V. Curri, F. Forghieri, Y. Yamamoto, T. Sasaki, and P. Poggiolini, "Ultra-long-haul transmission of 16x112 Gb/s spectrally-engineered DAC-generated Nyquist-WDM PM-16QAM channels with 1.05x(symbol-rate) frequency spacing," in *Proc. OFC2012* (Los Angeles, U.S.A., 2012).
5. J. Fickers, A. Ghazisaeidi, M. Salsi, G. Charlet, F. Horlin, P. Emplit, and S. Bigo, "Design rules for pulse shaping in PDM-QPSK and PDM-16QAM Nyquist-WDM coherent optical transmission systems," in *Proc. ECOC2012* (Amsterdam, The Netherlands, 2012).

6. W. Shieh and C. Athaudage, "Coherent optical orthogonal frequency division multiplexing," *IEEE Electron. Lett.* **42**(10), 587–589 (2006).
7. W. Shieh, X. Yi, Y. Ma, and Q. Yang, "Coherent optical OFDM: has its time come?" *J. Opt. Netw.* **7**(3), 234–255 (2008).
8. D. J. F. Barros and J. M. Kahn, "Optimized dispersion compensation using orthogonal frequency-division multiplexing," *J. Lightwave Technol.* **26**(16), 2889–2898 (2008).
9. F. Horlin, F. Quitin, J. Fickers, and P. Emplit, "Polarization division multiplexing for SC-FDE communications over dispersive optical fibers," in *Proc. IEEE Int. Conf. on Commun.* (Cape Town, South Africa, 2010).
10. S. Chandrasekhar and X. Liu, "Terabit superchannels for high spectral efficiency transmission," in *Proc. ECOC2010* (Torino, Italy, 2010).
11. T. Healy, F. G. Gunning, A. D. Ellis, and J. D. Bull., "Multi-wavelength source using low drive-voltage amplitude modulators for optical communications," *Opt. Express* **15**(6), 2981–2986 (2007).
12. Y. Ma, Y. Q. T. Yan, C. Simin, and W. Shieh, "1-Tb/s per channel coherent optical OFDM transmission with subwavelength bandwidth access," in *Proc. OFC2009* (Los Angeles, U.S.A., 2009).
13. A. Sano, E. Yamada, H. Masuda, E. Yamazaki, T. Kobayashi, E. Yoshida, Y. Miyamoto, R. Kudo, K. Ishihara, and Y. Takatori, "No-guard-interval coherent optical OFDM for 100-Gb/s long-haul WDM transmission," *J. Lightwave Technol.* **27**(16), 3705–3713 (2009).
14. S. Chandrasekhar and X. Liu, "Experimental investigation on the performance of closely spaced multi-carrier PDM-QPSK with digital coherent detection," *Opt. Express* **17**(24), 21,350–21,361 (2009).
15. B. L. Floch, M. Alard, and C. Berrou, "Coded orthogonal frequency division multiplex," *Proc. IEEE* **83**(6), 982–996 (1995).
16. C. Siclet and P. Siohan, "Design of BFDM/OQAM systems based on biorthogonal modulated filter banks," in *Proc. IEEE Globecom* (San Francisco, U.S.A., 2000).
17. D. S. Waldhauser and J. A. Nossek, "MMSE equalization for bandwidth efficient multicarrier systems," in *Proc. IEEE Int. Symp. on Circuits and Systems* (Island of Kos, Greece, 2006).
18. D. S. Waldhauser, L. G. Baltar, and J. A. Nossek, "MMSE subcarrier equalization for filter bank based multicarrier systems," in *Proc. IEEE Int. Workshop on Signal Process. Advances in Wireless Commun.* (Recife, Brazil, 2008).
19. M. Najjar, "Deliverable 4.2 - MIMO techniques and beamforming," Tech. rep., FP7-ICT PHYDYAS - PHYSical layer for DYNAMIC AccesS and cognitive radio (2010).
20. A. Ikhlef and J. Louveaux, "Per subchannel equalization for MIMO FBMC/OQAM systems," in *Proc. IEEE Pacific Rim Conf. on Commun., Computers and Signal Process.* (Victoria, Canada, 2009).
21. E. Kofidis and A. A. Rontogiannis, "Adaptive BLAST decision-feedback equalizer for MIMO-FBMC/OQAM systems," in *Proc. IEEE Personal, Indoor and Mobile Radio Commun.* (Istanbul, Turkey, 2010).
22. J. Zhao and A. D. Ellis, "Offset-QAM based coherent WDM for spectral efficiency enhancement," *Opt. Express* **19**(15), 14,617–14,631 (2011).
23. S. Randel, A. Sierra, X. Liu, S. Chandrasekhar, and P. J. Winzer, "Study of multicarrier offset-QAM for spectrally efficient coherent optical communications," in *Proc. ECOC2011* (Geneva, Switzerland, 2011).
24. A. Duel-Hallen, "Equalizers for multiple input/multiple output channels and PAM systems with cyclostationary input sequences," *IEEE J. Sel. Areas Commun.* **10**(3), 630–639 (1992).
25. A. Klein, G. K. Kaleh, and P. W. Baier, "Zero forcing and minimum mean-square-error equalization for multiuser detection in code-division multiple-access channels," *IEEE Trans. Vehicular Technol.* **45**(2), 276–287 (1996).

1. Introduction

In wavelength-division multiplexing (WDM) optical communication systems, increasing the spectral efficiency (SE) is a key target in order to respond to higher capacity requirements. The system designers have demonstrated the feasibility of significantly increasing the capacity on a single optical channel by using high-order modulation formats coupled with coherent detection at the receiver [1]. Advanced digital signal processing (DSP) solutions made possible thanks to the increasing speed of the new digital processors are designed to compensate for the impairments introduced by the optical fiber, like the chromatic dispersion (CD) and the polarization mode dispersion (PMD). The channel capacity is generally further doubled by transmitting independent signals on the two polarization axes of the optical field and by decoupling them at the receiver with additional signal processing (polarization division multiplexing - PDM) [2].

When multiple channels are considered together, the SE also strongly depends on the channel spacing, defined as the frequency separation between two optical carriers. As the communication channels suffer from inter-carrier interference (ICI) when the channel spacing is reduced

towards the symbol rate, substantial effort is currently devoted to design orthogonal multi-channel systems. Two approaches have been proposed in the literature to achieve this goal:

- The first approach, referred to as Nyquist wavelength-division multiplexing (N-WDM), consists in using nearly rectangular frequency pulses to limit the channel bandwidth to the symbol rate;
- The second approach, referred to as coherent orthogonal frequency-division multiplexing (CO-OFDM), results from the application of the OFDM modulation widely used for wireless communications systems to multiple optical channels.

N-WDM systems operate with shaping pulses having nearly rectangular frequency spectrum, of bandwidth equal to the symbol rate [3]. The class of root-raised-cosine (RRC) functions is of particular interest, because they satisfy the Nyquist criterion of zero inter-symbol interference (ISI) whatever the roll-off factor when applied at transmitter and receiver. Maximum SE can be achieved in case of zero roll-off factor, at zero ISI, if ideal conditions are met. However, N-WDM suffers from hardware implementation limitations such as the finite length of the pulse shaping filters, the timing jitter of the data sampling and the finite resolution of the analog/digital converters. These constraints translate into ISI and ICI, and therefore affect significantly the performance. Allowing for nonzero roll-off factors relaxes the constraints on the filter length and the tolerable jitter at expense of increasing ICI. Most recent works on N-WDM assume very small roll-off factors [4, 5].

The first implementations of OFDM for optical fibers are electrical per channel and aim at low computational complexity equalization of the channel impairments [6, 7]. OFDM divides the wideband channel in a set of narrowband flat subchannels that can be equalized independently with a single-tap equalizer. For the subchannels to be orthogonal, a redundant guard interval must be added to each block of symbols whose length has to be chosen carefully to prevent a too large capacity penalty [8]. OFDM is easily combined with multi-input multi-output (MIMO) techniques interesting to support PDM [9].

The implementation of optical OFDM is challenging as it requires the generation of a set of frequency-locked and synchronously modulated optical carriers (therefore the name CO-OFDM) [10]. Two alternative hardware architectures are considered to this end: the cascaded Mach-Zender modulator for small numbers of carriers [11] and the recirculating frequency shifter when the number of carriers is larger [12]. The frequency-locked carriers are separated by a wavelength demultiplexer, before being individually modulated by an IQ modulator, and combined by an optical coupler. In the case of CO-OFDM, the number channels remains generally small and the overhead incurred by the guard interval is too large. Paper [13] proposes to completely or partially remove the guard interval and to replace it with conventional per-channel DSP to cope with the resulting ICI. Minimum - but unfortunately not negligible - ICI arises when the channel spacing equals the symbol rate on each channel and when the symbols of the modulated channels are time-aligned as demonstrated experimentally in [14].

Filter-bank multi-carrier (FBMC) modulations, and more specifically OFDM-offset quadrature amplitude modulation (OQAM), are seen as an interesting alternative to OFDM for future communication systems [15, 16]. Like OFDM, OFDM-OQAM decomposes the communication channel in a set of lower-bandwidth subchannels that can therefore also be compensated at a low complexity with a single-tap equalizer. The time/frequency resolution of the waveforms is increased resulting in a better utilization of the physical resources and in an improved robustness to channel time variations and frequency offsets. Contrary to OFDM, OFDM-OQAM does not require the addition of a redundant guard interval and the created subchannels are only approximately flat and orthogonal. When the channel frequency selectivity increases, the OFDM-OQAM system suffers from both ISI and ICI, making it necessary to use advanced equalizer

structures [17, 18]. Furthermore the combination of OFDM-OQAM with MIMO techniques results in unmanageable inter-antenna interference (IAI) that prevents the straightforward application of the MIMO techniques designed for flat fading channels on each subchannel independently (as it was the case with OFDM) [19]. The MIMO extension of the equalizer structure [18] is proposed in [20] to deal with all sources of interference (ISI, ICI, IAI). While [20] focuses on linear and successive interference cancellation equalizers, paper [21] extends the results to the adaptive decision feedback equalizer.

Until now, the FBMC modulations have mainly been considered for wireless communications, even if first contributions highlight their interest for coherent optical fiber communications [22, 23]. Like CO-OFDM, OFDM-OQAM requires dedicated hardware to generate a set of frequency-locked and synchronously modulated optical carriers. Both [22, 23] simulate a single-polarization OFDM-OQAM system and demonstrate that it outperforms the N-WDM and CO-OFDM systems. This paper aims at demonstrating that it is possible to combine OFDM-OQAM and PDM to double the spectral efficiency. An equalizer similar to the one proposed in [20] is developed to decouple the two polarization signals. It works per subchannel at twice the symbol rate (DSP per optical subchannel) and is built taking the statistics of the interference coming from the two adjacent subchannels into account.

The paper is organized as follows. Section 2 describes the OFDM-OQAM system model. Section 3 develops the equivalent mathematical model, based on which the equalizer is developed in Section 4. Finally the performance and complexity of the proposed system is numerically assessed in Section 5. In the sequel, we use bold lowercase letters for the vectors and bold uppercase letters for the matrices. The operators $(\cdot)^T$ and $(\cdot)^H$ are used to denote the transpose and conjugate transpose of a vector or a matrix. Matrix $\mathbf{0}_{M,N}$ is the size- $M \times N$ matrix composed of zeros, matrix \mathbf{I}_N is the size- N identity matrix.

2. Dual-polarization OFDM-OQAM system

Figure 1 illustrates the model of the OFDM-OQAM system. The transmitter implements a synthesis filterbank composed of M channels, each modulated with QAM information symbols of variance σ_s^2 transmitted at the rate $1/T_s$. The information symbols are separated into their in-phase component $s_{(n_T,k)}^R[n]$ and quadrature component $s_{(n_T,k)}^I[n]$ (index $n_T = 1, 2$ refers to the two polarizations at the transmitter, index $k = 1, \dots, M$ refers to the M subchannels). The OQAM modulation is implemented by delaying the quadrature component by half a symbol with respect to the in-phase component (therefore the name offset QAM).

After upsampling to reach the sample rate $1/MT_s$ (the upsampling consists in inserting zeros between the samples of the input sequence), the symbols are convolved with the pulse shaping filter $u[n]$. Without loss of generality, we assume that the time domain impulse response of the pulse shaping filter $u[n]$ is a halfroot Nyquist filter (square root raised cosine filter). Two adjacent channels are spaced by a frequency shift equal to the input symbol rate. The model focuses on the channel k and its two adjacent channels $k-1$ and $k+1$ since the interference caused by the other channels on the channel k is negligible. In order to prevent inter-channel interference in the case of flat fading or slightly selective channels, a factor $\pm j$ multiplies the signal on the two adjacent channels. The M channels are added together after signal shifting on the frequency grid (multiplication with the exponentials at different frequencies).

The signal is transmitted through the frequency selective channel $h_{n_T,n_R}[n]$ representing the optical fiber and the transmit/receive front-ends (index n_R refers to the two polarizations at the receiver). Additive white Gaussian noise (AWGN) $w_{n_R}[n]$ of variance σ_w^2 corrupts the received signal.

At the receiver, the analysis filterbank implements the counter-part of each operation performed at the transmitter. After frequency shifting to process each channel around the origin,

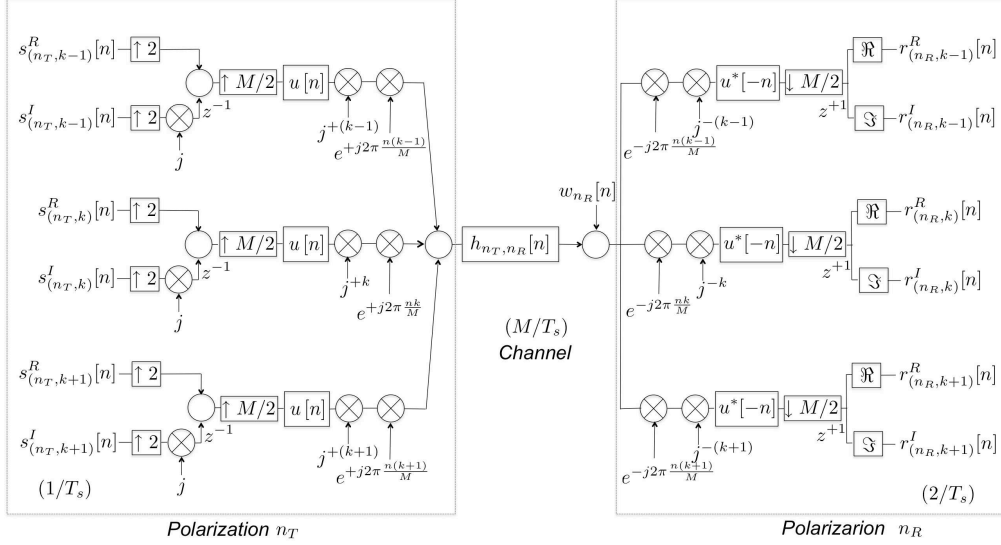


Fig. 1. OQAM-FBMC system model for subchannel k .

the received sequence is convolved with the filters matched to the pulse shaping filters. The half symbol delay applied on the imaginary branch is compensated so that both the real and imaginary sequences are received synchronously when downsampling.

3. Unified system model

The real output sequences $r_{(n_R, k)}^R[n]$ and $r_{(n_R, k)}^I[n]$ on the polarization n_R of channel k can be expressed as a function of the real input sequences $s_{(n_T, i)}^R[n]$ and $s_{(n_T, i)}^I[n]$ coming from both polarizations ($n_T = 1, 2$) of the channel k and its adjacent channels ($i = k - 1, k, k + 1$). Since we are developing the equalizer at twice the symbol rate, we need to define the polyphase components of the output sequences:

$$r_{(n_R, k), \rho}^R[n] = r_{(n_R, k)}^R[2n + \rho] \quad (1)$$

$$r_{(n_R, k), \rho}^I[n] = r_{(n_R, k)}^I[2n + \rho] \quad (2)$$

for $\rho = 0, 1$, so that the overall model is eventually working at the symbol rate:

$$\begin{aligned} r_{(n_R, k), \rho}^R[n] &= \sum_{n_T=1}^2 \sum_{i=k-1}^{k+1} g_{(n_T, i), (n_R, k), \rho}^{R, R}[n] \otimes s_{(n_T, i)}^R[n] \\ &+ \sum_{n_T=1}^2 \sum_{i=k-1}^{k+1} g_{(n_T, i), (n_R, k), \rho}^{I, R}[n] \otimes s_{(n_T, i)}^I[n] + v_{(n_R, k), \rho}^R[n] \end{aligned} \quad (3)$$

$$\begin{aligned} r_{(n_R, k), \rho}^I[n] &= \sum_{n_T=1}^2 \sum_{i=k-1}^{k+1} g_{(n_T, i), (n_R, k), \rho}^{R, I}[n] \otimes s_{(n_T, i)}^R[n] \\ &+ \sum_{n_T=1}^2 \sum_{i=k-1}^{k+1} g_{(n_T, i), (n_R, k), \rho}^{I, I}[n] \otimes s_{(n_T, i)}^I[n] + v_{(n_R, k), \rho}^I[n] \end{aligned} \quad (4)$$

where \otimes is the convolution operator. The parameter ρ is relative to the two polyphase components. The composite channel impulse responses result from the convolution of the transmitter

filter, channel response and receiver filter, downsampled by a factor M , as defined in:

$$g_{(n_T,i),(n_R,k),\rho}^{R,R}[n] := \Re\{p_i^R[m] \otimes h_{n_T,n_R}[m] \otimes q_k^R[m]\}_{|n=mM+\rho\frac{M}{2}} \quad (5)$$

$$g_{(n_T,i),(n_R,k),\rho}^{I,R}[n] := \Re\{p_i^I[m] \otimes h_{n_T,n_R}[m] \otimes q_k^R[m]\}_{|n=mM+\rho\frac{M}{2}} \quad (6)$$

$$g_{(n_T,i),(n_R,k),\rho}^{R,I}[n] := \Im\{p_i^R[m] \otimes h_{n_T,n_R}[m] \otimes q_k^I[m]\}_{|n=mM+\rho\frac{M}{2}} \quad (7)$$

$$g_{(n_T,i),(n_R,k),\rho}^{I,I}[n] := \Im\{p_i^I[m] \otimes h_{n_T,n_R}[m] \otimes q_k^I[m]\}_{|n=mM+\rho\frac{M}{2}} \quad (8)$$

in which the functions $p_i^R[n]$, $p_i^I[n]$ and $q_i^R[n]$, $q_i^I[n]$ are the synthesis and analysis filters:

$$p_i^R[n] := (j)^i \cdot u[n] \cdot \exp\left(j2\pi\frac{in}{M}\right) \quad (9)$$

$$p_i^I[n] := (-1)^i \cdot (j)^{i+1} \cdot u\left[n - \frac{M}{2}\right] \cdot \exp\left(j2\pi\frac{in}{M}\right) \quad (10)$$

and:

$$q_i^R[n] := (j)^{-i} \cdot u^*[-n] \cdot \exp\left(j2\pi\frac{in}{M}\right) \quad (11)$$

$$q_i^I[n] := (-1)^i \cdot (j)^{-i} \cdot u^*\left[-n - \frac{M}{2}\right] \cdot \exp\left(j2\pi\frac{in}{M}\right). \quad (12)$$

The synthesis and analysis filters are computed by first observing that the pulse shaping filter, the frequency shift and the factor $(j)^i$ on channel i can be combined in a unified impulse response $(j)^i \cdot u[n] \cdot \exp(j2\pi\frac{in}{M})$ at the transmitter and $(j)^{-i} \cdot u^*[-n] \cdot \exp(j2\pi\frac{in}{M})$ at the receiver.

At the transmitter, the real branch is only composed of the transmitter impulse response, giving directly Eq. (9). The imaginary branch is composed of the transmitter impulse response combined with the elements j and $z^{-M/2}$ (z^{-1} moved after the upsampling by $M/2$), giving Eq. (10) if we further note that $\exp\left(j2\pi\frac{i(n-M/2)}{M}\right) = \exp\left(j2\pi\frac{in}{M}\right) \cdot (-1)^i$.

At the receiver, the real branch is only composed of the receiver impulse response, giving directly Eq. (11). The imaginary branch is composed of the receiver impulse response combined with the factor $z^{M/2}$ (z^{+1} moved before the subsampling by $M/2$), giving Eq. (12) if we further note that $\exp\left(j2\pi\frac{i(n+M/2)}{M}\right) = \exp\left(j2\pi\frac{in}{M}\right) \cdot (-1)^i$.

The noise sequences $v_{(n_R,k),\rho}^R[n]$ and $v_{(n_R,k),\rho}^I[n]$ are obtained by filtering the input noise sequence $w_{n_R}[n]$ with the analysis filters, downsampling by M , keeping the real part or the imaginary part, and defining the polyphase components of the result as done in Eq. (1) and Eq. (2) for the received sequence.

In order to build a unified system model, the real/imaginary parts of the input sequences on both polarizations have been arranged in a sequence of length-4 vectors ($i = k-1, k, k+1$):

$$\mathbf{s}_i[n] := \left[(\mathbf{s}_{(1,i)}[n])^T \mid (\mathbf{s}_{(2,i)}[n])^T \right]^T \quad (13)$$

with:

$$\mathbf{s}_{(n_T,i)}[n] := \left[s_{(n_T,i)}^R[n] \mid s_{(n_T,i)}^I[n] \right]^T, \quad (14)$$

the real/imaginary parts of the noise and received sequence polyphase components on both polarizations have been arranged in sequences of length-8 vectors:

$$\mathbf{r}_k[n] := \left[(\mathbf{r}_{(1,k)}[n])^T \mid (\mathbf{r}_{(2,k)}[n])^T \right]^T \quad (15)$$

$$\mathbf{v}_k[n] := \left[(\mathbf{v}_{(1,k)}[n])^T \mid (\mathbf{v}_{(2,k)}[n])^T \right]^T \quad (16)$$

with:

$$\mathbf{r}_{(n_R,k)}[n] := \begin{bmatrix} r_{(n_R,k),0}^R[n] & r_{(n_R,k),1}^R[n] & r_{(n_R,k),0}^I[n] & r_{(n_R,k),1}^I[n] \end{bmatrix}^T \quad (17)$$

$$\mathbf{v}_{(n_R,k)}[n] := \begin{bmatrix} v_{(n_R,k),0}^R[n] & v_{(n_R,k),1}^R[n] & v_{(n_R,k),0}^I[n] & v_{(n_R,k),1}^I[n] \end{bmatrix}^T, \quad (18)$$

and the real/imaginary parts of the channel impulse responses corresponding to both polarizations are arranged in a sequence of size- 8×4 matrices:

$$\mathbf{G}_{i,k}[n] := \left[\begin{array}{c|c} \mathbf{G}_{(1,i),(1,k)}[n] & \mathbf{G}_{(2,i),(1,k)}[n] \\ \hline \mathbf{G}_{(1,i),(2,k)}[n] & \mathbf{G}_{(2,i),(2,k)}[n] \end{array} \right] \quad (19)$$

with:

$$\mathbf{G}_{(n_T,i),(n_R,k)}[n] := \begin{bmatrix} \mathcal{G}_{(n_T,i),(n_R,k),0}^{R,R}[n] & \mathcal{G}_{(n_T,i),(n_R,k),0}^{I,R}[n] \\ \mathcal{G}_{(n_T,i),(n_R,k),1}^{R,R}[n] & \mathcal{G}_{(n_T,i),(n_R,k),1}^{I,R}[n] \\ \mathcal{G}_{(n_T,i),(n_R,k),0}^{R,I}[n] & \mathcal{G}_{(n_T,i),(n_R,k),0}^{I,I}[n] \\ \mathcal{G}_{(n_T,i),(n_R,k),1}^{R,I}[n] & \mathcal{G}_{(n_T,i),(n_R,k),1}^{I,I}[n] \end{bmatrix}. \quad (20)$$

for $n_T, n_R = 1, 2$. Expressions (3)-(4) are equivalently written:

$$\mathbf{r}_k[n] = \sum_{i=k-1}^{k+1} \mathbf{G}_{i,k}[n] \otimes \mathbf{s}_i[n] + \mathbf{v}_k[n] \quad (21)$$

where the definition of the convolution \otimes of a vector sequence $\mathbf{x}[n]$ with a matrix sequence $\mathbf{G}[n]$ is traditionally defined as: $\mathbf{y}[n] := \sum_{m=-\infty}^{\infty} \mathbf{G}[m] \cdot \mathbf{x}[n-m]$.

4. Equalizer design

In the case of a single-polarization flat or slightly frequency selective channel, it can be shown that the interference caused by the subchannels $k-1$ and $k+1$ on the subchannel k is either imaginary on the real branch or real on the imaginary branch, so that no inter-subchannel interference is left when the real part (resp. the imaginary part) is selected on the real branch (resp. the imaginary branch). Furthermore, the convolution of the two halfroot Nyquist filters reduces to a Nyquist filter sampled at the symbol rate, so that the inter-symbol interference is removed on every subchannel. Therefore, a single-polarization slightly frequency selective channel can be compensated at a low complexity by simple inversion with a complex coefficient.

When the channel is significantly frequency selective, an equalizer must be foreseen to cope with the inter-symbol interference appearing on each subchannel, and with the inter-subchannel interference. In the case of a dual-polarized communication system, inter-polarization interference must also be taken into account in the equalizer design. The MIMO linear equalizer designed according to the minimum mean square error (MMSE) criterion can be built for the channel k based on the unified system model in Eq. (21). The derivation of the equalizer can be found in [24] for the continuous transmission case (infinite length equalizer computed in the z -domain) or in [25] for the burst transmission case (finite length equalizer computed based on a matrix model). Its application to the FBMC systems can be found in [18, 20].

For practical purposes, we focus in this paper on the finite length MMSE equalizer. A matrix model is obtained by assuming that the symbol vector $\mathbf{s}_k[n]$, at time n , is estimated based on the observation of the sequence of received vectors $\mathbf{r}_k[n]$ on the finite window $[n-W_2, n+W_1]$. The channel impulse responses are furthermore assumed of support limited to the interval $[-L_1, L_2]$. In this case, the convolution in the model in Eq. (21) can be expressed as a matrix product:

$$\bar{\mathbf{r}}_k[n] = \sum_{i=k-1}^{k+1} \bar{\mathbf{G}}_{i,k} \cdot \bar{\mathbf{s}}_i[n] + \bar{\mathbf{v}}_k[n] \quad (22)$$

where the symbol vector is defined as:

$$\bar{\mathbf{s}}_i[n] := [(\mathbf{s}_i[n + W_1 + L_1])^T \cdots (\mathbf{s}_i[n - W_2 - L_2])^T]^T, \quad (23)$$

the received and noise vectors are defined as:

$$\bar{\mathbf{r}}_k[n] := [(\mathbf{r}_k[n + W_1])^T \cdots (\mathbf{r}_k[n - W_2])^T]^T \quad (24)$$

$$\bar{\mathbf{v}}_k[n] := [(\mathbf{v}_k[n + W_1])^T \cdots (\mathbf{v}_k[n - W_2])^T]^T, \quad (25)$$

and the size $8(W_1 + W_2 + 1) \times 4(W_1 + L_1 + W_2 + L_2 + 1)$ channel matrix is defined as:

$$\bar{\mathbf{G}}_{i,k} := \begin{bmatrix} \mathbf{G}_{i,k}[-L_1] & \cdots & \mathbf{G}_{i,k}[L_2] & \mathbf{0}_{8 \times 2} & \cdots \\ \vdots & \ddots & \ddots & \ddots & \vdots \\ \cdots & \mathbf{0}_{8 \times 2} & \mathbf{G}_{i,k}[-L_1] & \cdots & \mathbf{G}_{i,k}[L_2] \end{bmatrix}. \quad (26)$$

The finite length linear MMSE equalizer that multiplies that received vector to produce the symbol estimate $\hat{\mathbf{s}}_k[n] = \mathbf{F}_k \cdot \bar{\mathbf{r}}_k[n]$ is given by [25]:

$$\mathbf{F}_k = \theta^H \cdot \left(\bar{\mathbf{G}}_{k,k}^H \cdot \mathbf{R}_{v_k v_k}^{-1} \cdot \bar{\mathbf{G}}_{k,k} + \mathbf{R}_{ss}^{-1} \right)^{-1} \cdot \bar{\mathbf{G}}_{k,k}^H \cdot \mathbf{R}_{v_k v_k}^{-1} \quad (27)$$

in which:

- The symbol auto-correlation matrix is an identity matrix:

$$\mathbf{R}_{ss} = \frac{\sigma_s^2}{2} \mathbf{I}_{4(W_1 + L_1 + W_2 + L_2 + 1)}, \quad (28)$$

because the symbols are independent.

- The noise auto-correlation matrix is:

$$\mathbf{R}_{v_k v_k} = \mathbf{R}_{vv} + \frac{\sigma_s^2}{2} \bar{\mathbf{G}}_{k-1,k} \cdot \bar{\mathbf{G}}_{k-1,k}^H + \frac{\sigma_s^2}{2} \bar{\mathbf{G}}_{k+1,k} \cdot \bar{\mathbf{G}}_{k+1,k}^H, \quad (29)$$

because the noise accounts for AWGN (first term) and for the second order statistics of the interference generated by channels $k - 1$ and $k + 1$ on channel k (two last terms). The AWGN auto-correlation matrix \mathbf{R}_{vv} includes coefficients expressing the correlation existing between two polyphase components of the noise sequences at the output of the receiver filter.

- The matrix θ is designed to select the symbol at time n in the vector $\bar{\mathbf{s}}_k[n]$:

$$\theta^H \cdot \bar{\mathbf{s}}_k[n] = \mathbf{s}_k[n]. \quad (30)$$

It is composed of zeros except on position $4(W_1 + L_1) + l$ in each column l ($l = 1, \dots, 4$) where it is 1.

The linear MMSE equalizer \mathbf{F}_k is a matrix of size $4 \times 8(W_1 + W_2 + 1)$ that can be viewed as a set of 4 size- $8(W_1 + W_2 + 1)$ filters applied to the received sequence. The variance of the error elements in $\boldsymbol{\varepsilon}_k[n] := \mathbf{s}_k[n] - \hat{\mathbf{s}}_k[n]$ can be found on the diagonal of the error auto-correlation matrix:

$$\mathbf{R}_{\boldsymbol{\varepsilon}_k \boldsymbol{\varepsilon}_k} = \theta^H \cdot \left(\bar{\mathbf{G}}_{k,k}^H \cdot \mathbf{R}_{v_k v_k}^{-1} \cdot \bar{\mathbf{G}}_{k,k} + \mathbf{R}_{ss}^{-1} \right)^{-1} \cdot \theta. \quad (31)$$

The MMSE linear equalizer is computed based on the knowledge of the channel impulse responses that is generally acquired through channel estimation. Another option is to employ adaptive algorithms that progressively converge to the MMSE solution based on the observation of the remaining symbol estimation error. The last solution also offers the advantage that the system is inherently robust to channel time variations. We believe however that this discussion is beyond the scope of the present paper.

5. Numerical results

The objective of this section is to assess the performance of the dual-polarized OFDM-OQAM system and to discuss its implementation feasibility. The numerical results are organized in three parts:

- We first investigate the gain achieved by making use of the OQAM modulation and dimension the MMSE equalizer.
- We secondly compare the performance and complexity of the OFDM-OQAM and N-WDM systems.
- We finally investigate the time and phase synchronization requirements at optical transmitters for the proper work of the OFDM-OQAM system.

If not stated differently, the numerical results are obtained for the following system parameters. The number of channels M is fixed to 8 in the simulations. The symbol rate per optical channel is equal to 30 Gsymb/s. The modulation format is offset quaternary phase shift keying (OQPSK). The transmit filter has a square root raised cosine (SRRC) pulse shape of 3-dB bandwidth equal to 30 GHz. Its length is equal to 8 symbols and its roll-off is equal to 1. The optical channel spacing is also equal to 30 GHz. Two independent symbol streams are transmitted on the two polarizations. In accordance to the scope of the paper focused on a dual polarization PDM system, the optical fiber model has been reduced to PMD. A 1000 km long typical standard single mode fiber, characterized by a $0.2 \text{ ps.km}^{-0.5}$ PMD, is assumed. The CD has been neglected in the simulations as it is generally pre-compensated digitally before equalization. The memory length of the 2×2 equalizer filters is fixed to $W_1 = 2W_2 = 20$ (see the explanations in the next section). The system performance is assessed by computing the (inverse of the) symbol estimation mean square error (MSE) or the bit error rate (BER) reached at the output of the equalizer. The results are averaged over 100 channel realizations.

5.1. OFDM-OQAM system parametrization

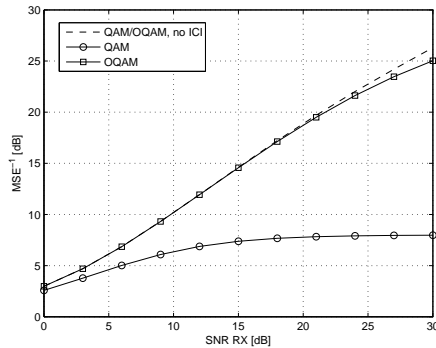


Fig. 2. Comparison of performance between the QAM and OQAM-FBMC systems for a varying SNR at the input of the receiver. The symbol rate, channel bandwidth and channel spacing are all equal to 30 Gsymb/s or GHz.

This subsection firstly evaluates the gain achieved by making use of the OQAM modulation compared to the conventional QAM modulation. Figure 2 compares the symbol estimation MSE of the QAM and OQAM-FBMC systems for a varying signal-to-noise ratio (SNR) at

the input of the receiver. While the dashed curve demonstrate that the performance of both QAM and OQAM-FBMC systems improves linearly with the SNR when the ICI is neglected (the interference coming from the adjacent sub-channels is null), the solid curves demonstrate that the OQAM modulation scheme significantly outperforms the QAM modulation scheme in the presence of ICI. The OQAM system performance in the presence of ICI is close to the performance in the absence of ICI. The QAM system performance in the presence of ICI saturates asymptotically to a low MSE value equal to -8 dB.

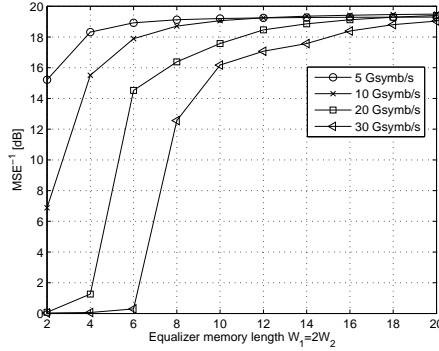


Fig. 3. Performance of the OFDM-OQAM system as a function of the equalizer memory length for a varying symbol rate. The channel bandwidth and channel spacing are varying according to the symbol rate. The received SNR is fixed to 20 dB.

Figure 3 evaluates the performance/complexity trade-off for the OFDM-OQAM system. It illustrates the symbol estimation MSE of the OQAM system as a function of the equalizer memory lengths W_1, W_2 for different values of the symbol rate. The memory lengths L_1, L_2 account for the anti-causal and causal parts respectively of the composite impulse response. In our simulations, we assume that L_1 is equal to the half length of the combined transmit/receive filters (therefore $L_1 = 8$) and that L_2 is equal to the remaining half length of the combined transmit/receive filters plus the length of the optical fiber impulse response (therefore $L_2 = 8 + L_{of}$ where L_{of} is the length of the optical fiber impulse response equal to 2, 5, 10, 15 when $R_s = 5, 10, 20, 30$ Gsym/s respectively). When the equalizer is designed, the length W_1 represents the observation span on the indices above n where the symbol vector $s_k[n]$ contributes due to the causal part of the impulse response, and the length W_2 represents the observation span on the indices below n where the symbol vector $s_k[n]$ contributes due to the anti-causal part of the impulse response. It is therefore reasonable to select $W_1 > W_2$ to estimate the symbol vector $s_k[n]$ and we choose $W_1 = 2W_2$. The pulse shaping filter 3-dB bandwidth and the channel spacing are adjusted according to the symbol rate. The SNR is fixed to 20 dB. When the symbol rate increases (or equivalently the channel bandwidth), the channel frequency selectivity on each channel becomes significant and the necessary equalizer memory length to cope with the ISI increases. However, this is partly compensated from a complexity point-of-view by the number of channels that decreases with the channel bandwidth if the overall communication bandwidth is maintained constant. Assuming a 30 Gsym/s symbol rate, the equalizer should be of memory length at least equal to 20 to ensure a negligible degradation.

5.2. Performance comparison with N-WDM

This subsection targets to compare the proposed OFDM-OQAM system to the well investigated N-WDM system. The N-WDM system is simulated by reducing the roll-off of the conventional

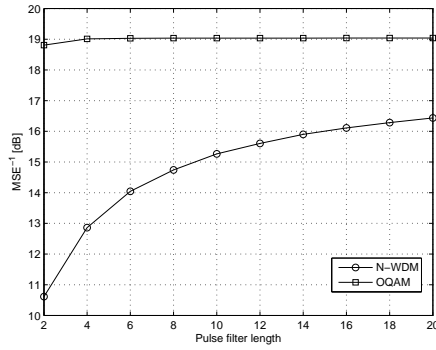


Fig. 4. Comparison of performance between the N-WDM and OQAM systems for a varying pulse length. The received SNR is fixed to 20 dB.

QAM system to 0.05. In a first step, we keep the channel spacing equal to the symbol rate so that both systems deliver the same spectral efficiency. Figure 4 illustrates the symbol estimation MSE as a function of the pulse shaping filter length, and therefore of its implementation computational complexity. The SNR is equal to 20 dB. The adjacent channels in the case of the OFDM-OQAM system remain orthogonal whatever their frequency overlap, explaining the constant performance as a function of the pulse shaping length. In the case of the N-WDM system, the frequency overlap between the adjacent channels strongly impacts the performance. The performance improves significantly with the pulse shaping length and tends asymptotically to a value lower than the one obtained with the OFDM-OQAM system, because the roll-off factor different from zero still lets a small amount of inter-channel interference.

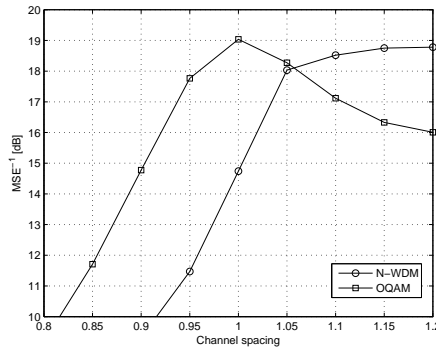


Fig. 5. Comparison of performance between the N-WDM and OQAM systems for a varying subchannel spacing (normalized to the symbol rate equal to 30 Gsymb/s). The received SNR is fixed to 20 dB.

In a second step, we keep the pulse shaping length constant and vary the channel spacing. Figure 5 illustrates the symbol estimation MSE of both OFDM-OQAM and N-WDM systems as a function of the channel spacing normalized to the symbol rate. The SNR is fixed to 20 dB. While the performance of the N-WDM system continuously improves with the channel spacing since the ICI is reduced in that case, the performance of the OFDM-OQAM system is optimal for a channel spacing equal to the symbol rate since the channels are orthogonal in that case.

We observe the large performance gain obtained with the OQAM modulation scheme in the presence of ICI. The N-WDM system outperforms the OQAM system when the ICI becomes negligible for large channel spacings but this is at the expense of spectral efficiency!

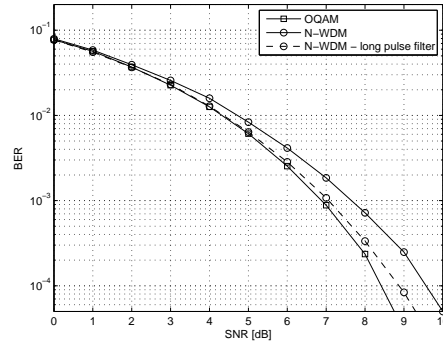


Fig. 6. Comparison of performance between the N-WDM and OQAM systems for a pulse length equal to 8 or 20 (long pulse filter).

Figure 6 illustrates the BER as a function of the SNR for both OFDM-OQAM and N-WDM systems. As for the N-WDM system, two values of the pulse shaping length are considered. The BER analysis confirms the former conclusions: the OFDM-OQAM system outperforms the N-WDM system when the spectral efficiency is equal for both systems, the performance of this last scheme can be improved - but do not reach the performance of the OFDM-OQAM system - by increasing the length of the pulse shaping filter (or equivalently its implementation complexity).

5.3. Impact of synchronization errors

The improved performance achieved with the OFDM-OQAM system comes unfortunately at the cost of important synchronization requirements at the transmit side: the phase of the optical carriers should necessarily be shifted by $\pi/2$ between the adjacent channels; the pulse shaping filters should be time aligned on all channels. This subsection investigates the impact of synchronization errors on the BER performance.

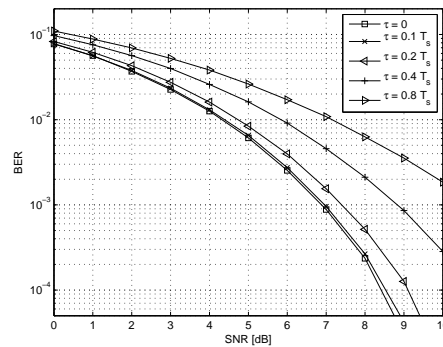


Fig. 7. Impact of a time synchronization error on the OQAM system bit error rate.

Figure 7 gives the BER as a function of the SNR for increasing values of the time synchronization error. The time error τ is simulated as a uniformly distributed random variable of maximum indicated in the figure. Figure 8 on the other hand gives the BER as a function

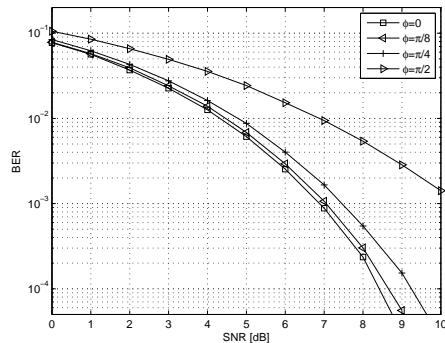


Fig. 8. Impact of a phase synchronization error on the OQAM system bit error rate.

of the SNR for increasing values of the phase synchronization error. Like the time error, the phase error ϕ is assumed to be a uniformly distributed random variable of maximum indicated in the figure, constant for each channel realization. Even if phase/time synchronization errors clearly degrade the BER performance, it is noteworthy that the performance is still acceptable for significant errors: a $0.1 T_s$ time error or a $\pi/8$ phase error are affordable.

6. Conclusion

This paper demonstrates that the OFDM-OQAM modulation recently proposed for coherent optical fiber communications can advantageously be combined with PDM to still double the spectral efficiency. More specifically, the MMSE equalizer working per channel at twice the symbol rate is designed to decouple the two polarization signals, and its efficiency is assessed numerically. Compared to the well studied N-WDM system, the proposed system benefits from an improved BER performance when the pulse shaping filters are of identical length, or equivalently from a reduced computational complexity to achieve an identical BER. The main challenge in the design of the OFDM-OQAM system comes from the necessary time and phase synchronization of the optical channels, but we demonstrate that the synchronization requirements are actually not stringent.